Biochemical and structural characterization of residue 96 mutants of Plasmodium falciparum triosephosphate isomerase: Active-site loop conformation, hydration and identification of...

Article *in* Acta Crystallographica Section D Biological Crystallography · September 2009

DOI: 10.1107/S0907444909018666 · Source: PubMed

CITATIONS
14

READS
137

6 authors, including:

Mousumi Banerjee
Indian Institute of Science Education and Research, Tirupati
16 PUBLICATIONS **158** CITATIONS
SEE PROFILE

Padmanabhan Balaram
Indian Institute of Science
595 PUBLICATIONS **19,813** CITATIONS
SEE PROFILE

Mathur R N Murthy
Indian Institute of Science
188 PUBLICATIONS **3,661** CITATIONS
SEE PROFILE

Acta Crystallographica Section D
Biological Crystallography
ISSN 0907-4449

Biochemical and structural characterization of residue 96 mutants of *Plasmodium falciparum* triosephosphate isomerase: active-site loop conformation, hydration and identification of a dimer-interface ligand-binding site

P. Gayathri,[a] Mousumi Banerjee,[a] A. Vijayalakshmi,[a] Hemalatha Balaram,[b] P. Balaram[a] and M. R. N. Murthy[a]*

[a]Molecular Biophysics Unit, Indian Institute of Science, Bangalore 560 012, India, and [b]Molecular Biology and Genetics Unit, Jawaharlal Nehru Centre for Advanced Scientific Research, Jakkur, Bangalore 560 064, India

Correspondence e-mail: mrn@mbu.iisc.ernet.in

Received 23 March 2009
Accepted 17 May 2009

PDB References: PfTIM, F96S mutant, 2vfd, r2vfdsf; F96S mutant, complex with 3PG, 2vfe, r2vfesf; F96H mutant, 2vff, r2vffsf; F96H mutant, complex with 3PG, 2vfg, r2vfgsf; F96W mutant, complex with 3PG, 2vfh, r2vfhsf; wild type, complex with 3PG, 2vfi, r2vfisf.

Plasmodium falciparum TIM (PfTIM) is unique in possessing a Phe residue at position 96 in place of the conserved Ser that is found in TIMs from the majority of other organisms. In order to probe the role of residue 96, three PfTIM mutants, F96S, F96H and F96W, have been biochemically and structurally characterized. The three mutants exhibited reduced catalytic efficiency and a decrease in substrate-binding affinity, with the most pronounced effects being observed for F96S and F96H. The k_{cat} values and K_m values are $(2.54 \pm 0.19) \times 10^5$ min^{-1} and 0.39 ± 0.049 mM, respectively, for the wild type; $(3.72 \pm 0.28) \times 10^3$ min^{-1} and 2.18 ± 0.028 mM, respectively, for the F96S mutant; $(1.11 \pm 0.03) \times 10^4$ min^{-1} and 2.62 ± 0.042 mM, respectively, for the F96H mutant; and $(1.48 \pm 0.05) \times 10^5$ min^{-1} and 1.20 ± 0.056 mM, respectively, for the F96W mutant. Unliganded and 3-phosphoglycerate (3PG) complexed structures are reported for the wild-type enzyme and the mutants. The ligand binds to the active sites of the wild-type enzyme (wtPfTIM) and the F96W mutant, with a loop-open state in the former and both open and closed states in the latter. In contrast, no density for the ligand could be detected at the active sites of the F96S and F96H mutants under identical conditions. The decrease in ligand affinity could be a consequence of differences in the water network connecting residue 96 to Ser73 in the vicinity of the active site. Soaking of crystals of wtPfTIM and the F96S and F96H mutants resulted in the binding of 3PG at a dimer-interface site. In addition, loop closure at the liganded active site was observed for wtPfTIM. The dimer-interface site in PfTIM shows strong electrostatic anchoring of the phosphate group involving the Arg98 and Lys112 residues of PfTIM.

1. Introduction

Triosephosphate isomerase (TIM), which is a central enzyme of the glycolytic pathway, catalyzes the interconversion of dihydroxyacetone phosphate (DHAP) and glyceraldehyde 3-phosphate (GAP) *via* an enediolate intermediate (Albery & Knowles, 1977; Rose, 1962). The enediol phosphate intermediate is critically poised to undergo competing reactions: isomerization to the aldehyde on one hand and phosphate elimination to yield the toxic metabolite methylglyoxal on the other (Richard, 1991). The efficiency with which TIM catalyses isomerization has led to many incisive studies dissecting the mechanism of the reaction (Alber *et al.*, 1987; Albery & Knowles, 1976*a*,*b*,*c*, 1977; Knowles, 1991; Rieder & Rose, 1959). Extensive studies led Jeremy Knowles to famously describe TIM as an evolutionarily 'perfect' enzyme (Albery & Knowles, 1976*a*,*b*,*c*).

Studies on TIM have been central to the development of our understanding of the role of protein dynamics in modulating catalytic function (Alber *et al.*, 1981; Sun & Sampson, 1998, 1999; Joseph *et al.*, 1990; Derreumaux & Schlick, 1998). In TIM, loop 6, which consists of an 11-residue polypeptide segment, moves as a rigid body about flanking hinge residues and closes over the active site, resulting in two distinct conformational states: the 'loop-open' and the 'loop-closed' states of the enzyme (Alber *et al.*, 1987; Joseph *et al.*, 1990). Loop closure has been suggested to be important in preventing the undesired phosphate-elimination process, thereby facilitating the competing isomerization reaction (Pompliano *et al.*, 1990). The large body of crystallographic information on the TIM structure suggests that ligand occupancy at the active site results in selection of the loop-closed conformation. The loop has been observed in the open state in the absence of the ligand and in the closed state in the presence of the ligand in the majority of crystal structures, with a few exceptions. In one of the subunits of a crystal form of rabbit TIM the loop is in a closed state in the absence of the ligand (Aparicio *et al.*, 2003), while in *Trypanosoma brucei* TIM complexed with *N*-hydroxy-4-phosphono-butanamide (Verlinde *et al.*, 1992) and many *Plasmodium falciparum* TIM (PfTIM) structures (Parthasarathy, Balaram *et al.*, 2002) the loop occurs in an open conformation in the presence of the ligand. However, investigation of loop dynamics using NMR has shown that the loop motion is not ligand-gated (Williams & McDermott, 1995). Hence, it was concluded that there is a conformational heterogeneity in TIM; the loop opens and closes over the active site irrespective of the presence of the ligand and the equilibrium tilts in favour of the loop-closed state in the presence of the ligand (Rozovsky *et al.*, 2001; Rozovsky & McDermott, 2001).

While investigating PfTIM, we repeatedly encountered ligand-bound structures in which loop 6 adopted the open conformation (Parthasarathy, Balaram *et al.*, 2002; Parthasarathy, Ravindra *et al.*, 2002; Parthasarathy *et al.*, 2003). In the structure of PfTIM complexed with phosphoglycolic acid (PGA; PDB code 1lyx), the loop is closed (Parthasarathy, Ravindra *et al.*, 2002). In one of the subunits of PfTIM complexed with 2-phosphoglycerate (2PG; PDB code 1o5x) the loop occurs in both closed and open conformations, with occupancies of 0.6 and 0.4, respectively (Parthasarathy *et al.*, 2003). Inspection of the available sequences of TIM revealed that residue 96, which is proximal to the active site, is Ser in majority of organisms, with *P. falciparum* being one of the very few exceptions. Of the 412 available unique TIM sequences in the SWISS-PROT database (June 2008), 406 sequences have Ser at position 96, one plasmodial sequence has Phe (Q07412), three listeria sequences have Ala (Q71WW9, Q8Y4I3, Q92EU4), *Ehrlichia chaffeensis* (strain Arkansas, Q2GGH7) has Tyr and *Baumannia cicadellinicola* subsp. *Homalodisca coagulata* (Q1LTT4) has Ile. Among TIMs with available crystal structures, PfTIM, with Phe at position 96, is the only exception. Fig. 1 shows a partial alignment of the sequences of TIMs for which crystal structures are currently available and highlights the conservation of Ser96 in all cases except *P. falciparum*. Indeed, in a review of the structural biochemistry of TIM published many years ago when all available sequences had Ser at position 96, Alber and coworkers noted that 'the role of the conserved Ser96 is a mystery' (Alber *et al.*, 1987). The crystal structure of the S96P mutant of chicken TIM revealed changes in the water structure in the active-site cavity, suggesting a role for water in the catalytic activity of TIM (Zhang *et al.*, 1999).

Inspection of PfTIM crystal structures suggested that the enhanced propensity for the loop-open conformation may be a consequence of the unfavourable interaction between the side chains of Phe96 and Ile170 in the loop-closed form (Parthasarathy, Balaram *et al.*, 2002). However, observation of the loop-closed conformation in the PfTIM–phosphoglycolate complex (PDB code 1lyx; Parthasarathy, Ravindra *et al.*, 2002) reveals that side-chain reorientation of Phe96 and Leu167 can indeed permit loop closure.

In order to probe the role of residue 96, we have constructed F96S, F96H and F96W mutants of PfTIM. The first of these mutations changes the residue to that of most TIM sequences, while the other two mutations result in cyclic side chains as in Phe. The results described in this report establish a significant loss of catalytic activity for the F96S and F96H mutants, while F96W is substantially active. Analysis of the kinetic parameters of the mutants shows a significant reduction in ligand binding affinity for the F96S and F96H mutants. Crystallographic studies of the mutants with and without the ligand 3-phosphoglycerate (3PG) reveal extensive differences in active-site hydration in the F96S and F96H mutants, suggesting a connection to the impaired catalytic activity. The serendipitous observation of a second ligand binding site located at the dimer interface on soaking of crystals of the enzyme in 3PG solution reveals protein–inhibitor interactions involving the phosphate group which differ distinctly from those at the active site.

2. Materials and methods

2.1. Cloning, expression and purification

The *P. falciparum* triosephosphate isomerase gene was cloned into pTrc99A vector and called pARC1008 (Ranie *et al.*, 1993). The protein was overexpressed in *Escherichia coli* strain AA200, which has a null mutation for the host TIM gene (Anderson & Cooper, 1970). Four mutants of PfTIM were constructed by site-directed mutagenesis using the megaprimer PCR method (Sarkar & Sommer, 1990). The mutagenesis primers are 5′-TCTTCTTTCAGAA**TGGCCA**-AT-3′ for F96S, 5′-TCTTCTTTCATGA**TGGCCA**ATAATA-AC-3′ for F96H and 5′-TCTTCTTTCCCAA**TGGCCA**ATA-ATAAC-3′ for F96W. (The restriction site for *Hae*III introduced into each primer is shown in bold.) The wild-type PfTIM gene was used as the template for the F96S, F96H and F96W mutants. The wild-type and mutant constructs were transformed into AA200 cells and inoculated into Terrific broth for protein expression. Induction was carried out at 303 K for 12 h. The purification of TIM involved a two-step

protocol. In the first step, the cell lysate was subjected to ammonium sulfate precipitation at 40 and 80% saturation. TIM could be selectively precipitated at 75–80% saturation. The protein was further purified by gel filtration (Sephacryl-200 column) and ion-exchange chromatography (HR 75, Q-Sepharose) on an ÄKTA Basic FPLC system. The purified protein was stored at a concentration of 1 mg ml^{-1} in 20 m*M* Tris–HCl pH 8.0 containing 2 m*M* DTT at 277 K and characterized by SDS–PAGE.

The mutations were confirmed using electrospray ionization mass spectrometry (Table 1) and DNA sequencing. Electrospray ionization mass spectra were recorded on an HP (Agilent) electrospray mass spectrometer linked to a 1100 series HPLC. The electrospray was carried out using a capillary with an internal diameter of 0.1 mm. The tip was held at 5000 V in a positive-ion detection mode. Nebulization was assisted by N_2 gas (99.8%) at a flow rate of 10 l min^{-1}. The spray chamber was maintained at 573 K. The ion optics zone was optimized for maximal ion transmission and a declustering potential (fragmentor voltage) of 200 V was set for detection. Data were acquired across a suitable mass range using a conventional quadrupole with cycle time of 3 s. The spectrometer was tuned to five calibration standards provided by the manufacturer. Data processing was performed using the deconvolution module of the *ChemStation* software to detect the multiple charge states and obtain derived masses.

2.2. Enzyme activity

The TIM enzyme activity was determined by the conversion of GAP (glyceraldehyde 3-phosphate) to DHAP (dihydroxyacetone phosphate) in the presence of TIM and α-glycerol phosphate dehydrogenase (Oesper & Meyerhof, 1950; Plaut & Knowles, 1972). The enzymes were freshly prepared in 100 m*M* triethanolamine–HCl (TEA) pH 7.6. The reaction mixture contained (in a final volume of 1 ml) 100 m*M* TEA, 5 m*M* EDTA, 0.5 m*M* NADH, 20 µg ml^{-1} α-glycerol phosphate dehydrogenase and 0.16–2.4 m*M* glyceraldehyde 3-phosphate. The enzyme activity was determined by monitoring the decrease in absorbance at 340 nm. The dependence of the initial rate on the substrate concentration was analyzed according to the Michaelis–Menten equation. The inhibition constant, K_i, of 3-phosphoglycerate (3PG) was obtained by analyzing the effect of the inhibitor on the initial velocity of the conversion of glyceraldehyde 3-phosphate. The concentration range used for 3PG (disodium salt, Sigma Chemicals) was from 0.5 to 4.0 m*M*. Inhibition constants were obtained from the negative intercept on the *x* axis of a plot of the apparent K_m *versus* the inhibitor concentration. The values of the kinetic parameters (K_m, k_{cat}) were calculated from Lineweaver–Burke plots.

2.3. Crystallization, data collection and refinement

The PfTIM mutants were purified as described above and concentrated to approximately 10 mg ml^{-1}. For cocrystallization attempts with the ligand 3PG (disodium salt, Sigma Chemicals), the protein was incubated with a 100-fold molar excess of the ligand for approximately 5 h prior to setting up crystallization. Crystals were obtained using the conditions reported for the crystallization of PfTIM (Parthasarathy, Balaram *et al.*, 2002), with a crystallization cocktail containing 0.1 *M* sodium acetate pH 4.0–5.5 and polyethylene glycol 1450 (Sigma Chemicals) varying from 8% to 24% in the reservoir. The hanging drop contained 3 µl protein with 3 µl crystallization cocktail and the reservoir buffer contained 500 µl crystallization cocktail. Crystals appeared within 2 d and grew to the required size within 4–5 d. Reservoir buffer with 20% glycerol was used as a cryoprotectant before flash-freezing the crystal in liquid nitrogen. For soaking experiments, the crystals were soaked in 10 µl reservoir buffer containing 100 m*M* ligand and 20% glycerol as a cryoprotectant. X-ray diffraction data were collected using a Rigaku rotating-anode X-ray generator and a MAR Research image-plate detector system. A data set for the F96S mutant cocrystallized with 3PG was collected at a wavelength of 0.93 Å on synchrotron beamline BL44XU at SPring-8, Hyogo, Japan using a DIP-2040b image-plate detector. The data-collection statistics for all data sets are shown in Table 2.

The 1.1 Å PfTIM crystal structure (PDB code 1o5x) was used as a model for the structure determination of the mutants and their complexes. The coordinates of 1o5x were modified by removing the loop 6 residues, ligand, water molecules and alternate conformations. For all crystals isomorphous with 1o5x, difference density maps were calculated using the corresponding data. Molecular replacement was run using *MOLREP* from the *CCP*4 package (Collaborative Computational Project, Number 4, 1994) with 1o5x, modified as above, as the model for the F96H mutant and for the wild-type enzyme after soaking in 3PG. Refinements of all the models

```
                    90        100       110
P.fal   EIAKDLNIEYVIIGHFERRKYFHETDEDVRE
L.mex   PILKDIGVHWVILGHSERRTYYGETDEIVAQ
T.cru   QILKDYGISWVVLGHSERRLYYGETNEIVAE
T.bru   PILKDFGVNWIVLGHSERRAYYGETNEIVAD
G.lam   EMLQDMGLKHVIVGHSERRRIMGETDEQSAK
Human   GMIKDCGATWVVLGHSERRHVFGESDELIGQ
Yeast   DQIKDVGAKWVILGHSERRSYFHEDDKFIAD
Rabbit  GMIKDCGATWVVLGHSERRHVFGESDELIGQ
Chick   AMIKDIGAAWVILGHSERRHVFGESDELIGQ
C.ele   AMIKDLGLEWVILGHSERRHVFGESDALIAE
E.his   GMLVDCQVPYVILGHSERRQIFHESNEQVAE
E.col   AMLKDIGAQYIIIGHSERRTYHKESDELIAK
V.mar   AMLKEFGATHIIIGHSERREYHAESDEFVAK
T.tenc  AMIKDVGADWVILGHSERRQIFGESDELIAE
T.the   RMLSDLGCRYAIVGHSERRRYHGETDALVAE
B.ste   VMLKDLGVTYVILGHSERRQMFAETDETVNK
T.mar   LMLQEIGVEYVIVGHSERRRIFKEDDEFINR
T.ten   ENIKEAGGSGVILNHSEAP....LKLNDLAR
P.woe   EAVKEAGAVGTLLNHSENR....MILADLEA
M.jan   EAIKDCGCKGTLINHSEKR....MLLADIEA
                        ▲
```

Figure 1
A section of the structure-based sequence alignment of TIMs of known structure. The position corresponding to Phe96 of PfTIM is highlighted in grey and marked by a triangle. The sequence numbering at the top corresponds to PfTIM. The alignment was obtained using *MUSTANG* (Konagurthu *et al.*, 2006) and represented using *ESPript* (Gouet *et al.*, 1999).

Table 1
Characterization of the F96 mutants.

Protein	Expected mass† (Da)	Observed mass (Da)	K_m, GAP‡ (m*M*)	k_{cat}§ (min^{-1})	k_{cat}/K_m (min^{-1} mM^{-1})	K_i, 3PG (m*M*)	Ratio of k_{cat}/K_m (mutant/WT)
WT	27831.0	27829.8	0.39 ± 0.049	(2.54 ± 0.19) × 10^5	6.51 × 10^5	1.9 ± 0.5	1
F96S	27771.4	27770.6	2.18 ± 0.028	(3.72 ± 0.28) × 10^3	1.71 × 10^3	>5	0.0026
F96H	27821.5	27821.4	2.62 ± 0.042	(1.11 ± 0.03) × 10^4	4.23 × 10^3	>5	0.0064
F96W	27870.6	27869.0	1.20 ± 0.056	(1.48 ± 0.05) × 10^5	1.23 × 10^5	>5	0.1889

† The expected mass for the wild type and mutants was calculated with Val at position 163. ‡ The K_m values for yeast and chicken TIM are 1.27 ± 0.06 m*M* (Kreitsch *et al.*, 1970) and 0.47 m*M* (Putman *et al.*, 1972), respectively. § The k_{cat} values for yeast and chicken TIM are 1 × 10^6 min^{-1} (Kreitsch *et al.*, 1970) and 2.56 × 10^5 min^{-1} (Putman *et al.*, 1972), respectively.

Table 2
Crystallographic data-collection statistics.

Values in parentheses are for the last resolution shell.

	F96S, unliganded	F96H, unliganded	F96S, liganded	F96H, liganded	WT–3PG, loop closed	F96W, liganded
Space group	$P2_1$	$P2_1$	$P2_1$	$P2_1$	$P2_1$	$P2_1$
Unit-cell parameters						
a (Å)	53.5	53.4	53.8	90.2	53.6	53.5
b (Å)	50.7	50.7	50.8	47.1	51.1	51.1
c (Å)	89.1	89.1	87.0	109.1	92.1	86.5
β (°)	92.3	92.2	92.5	96.6	98.2	92.4
Resolution range (Å)	50–1.4 (1.45–1.4)	50–1.7 (1.76–1.7)	50–2.2 (2.8–2.2)	50–1.95 (2.02–1.95)	50–2.25 (2.33–2.25)	50–2.0 (2.07–2.0)
No. of unique reflections	90838	49710	23622	62256	22598	31777
Redundancy	3.3 (3.2)	2.3 (2.1)	2.9 (2.1)	2.7 (2.0)	2.5 (1.8)	3.0 (2.7)
Completeness (%)	96.3 (93.9)	93.8 (81.2)	97.6 (87.3)	93.3 (82.3)	95.1 (80.5)	99.6 (98.7)
R_{merge}†	5.2 (23.8)	5.2 (23.4)	9.0 (41.5)	9.8 (44.2)	9.6 (38.2)	8.0 (42.1)
$\langle I/\sigma(I)\rangle$	40.5 (7.0)	20.1 (4.4)	10.6 (1.9)	9.8 (1.9)	9.2 (2.3)	13.5 (2.4)

† $R_{merge} = \sum_{hkl}\sum_i |I_i(hkl) - \langle I(hkl)\rangle| / \sum_{hkl}\sum_i I_i(hkl)$, where $I_i(hkl)$ is the *i*th observation of $I(hkl)$ and $\langle I(hkl)\rangle$ is its mean intensity.

were carried out using *REFMAC*5 (Murshudov *et al.*, 1997) and the loop 6 residues, ligand and water molecules were added on the basis of $2F_o - F_c$ and $F_o - F_c$ difference density maps contoured at 1σ and 3σ, respectively. Model building was performed using *Coot* (Emsley & Cowtan, 2004). A simulated-annealing omit map (Brunger *et al.*, 2007) for the ligand and the neighbouring water molecules was calculated using *CNS* v.1.2 (Brunger, 2007). The *B* factors of all the atoms were also refined and alternate conformations were included wherever necessary.

2.4. Structure analysis

All structural superpositions were carried out by secondary-structure matching (Krissinel & Henrick, 2004) using *Coot*. Hydrogen bonds and van der Waals contacts were identified using the *CONTACT* program of the *CCP*4 suite based on distance criteria of 3.5 and 4.0 Å, respectively. The figures were generated using *PyMOL* (DeLano, 2002). The program *VOIDOO* (Kleywegt & Jones, 1994) was used for the estimation of cavity volumes in the native PfTIM structure.

2.5. PDB accession codes

The coordinates and structure factors of the crystal structures have been submitted to the Protein Data Bank and the structures have been assigned the accession codes 2vfd, 2vfe, 2vff, 2vfg, 2vfh and 2vfi for the F96S mutant and its complex with 3PG, the F96H mutant and its complex with 3PG, the F96W mutant complexed with 3PG and wild-type PfTIM with 3PG bound at the active site and interface, respectively.

3. Results

3.1. Enzyme kinetics

Table 1 summarizes the kinetic parameters determined for the wild-type *P. falciparum* enzyme and the three position 96 mutants. The F96S and F96H mutants show a dramatic reduction in k_{cat} and an increase in K_m. The F96W mutant exhibits an activity close to that of the wild type, with a k_{cat} value of (1.48 ± 0.05) × 10^5 min^{-1} compared with (2.54 ± 0.19) × 10^5 min^{-1} for the wild type. Notably, the F96W mutant possesses a much higher catalytic activity compared with the F96S and F96H mutants, although there is a moderate reduction relative to the wild type. There is also a decrease in the affinity for 3PG for all of the mutants.

3.2. Crystal structures

All of the structures have been refined to reasonable R_{work} and R_{free} values and good geometry (Table 3). The presence of the mutation was confirmed by DNA sequencing, by mass spectrometry (Table 1) and by examining the electron density at position 96 in the F96S, F96H and F96W mutant structures. Crystallization of the F96S and F96H mutants in the presence of 50 m*M* 3PG yielded crystals of diffraction quality. The electron-density map revealed that the active site was unliganded, with loop 6 in the open conformation (Table 4),

Table 3
Refinement statistics.

	F96S, unliganded	F96H, unliganded	F96S, liganded	F96H, liganded	WT–3PG, loop closed	F96W, liganded
Resolution range (Å)	50–1.4	50–1.7	50–2.2	50–1.95	50–2.25	50–2.0
R factor† (%)	18.9	20.5	20.7	19.5	17.9	19.1
R_{free}† (%)	20.7	22.8	26.7	23.8	23.2	24.0
Model quality						
No. of atoms						
Protein	3951	4020	3906	7810	3956	4064
Water	643	482	267	662	349	426
Ligand						
3PG	—	—	22	44	44	22
Glycerol	—	—	12	—	—	—
Sulfate	5	—	—	—	—	—
Average *B* factor (Å^2)						
Protein	14.5	19.5	34.2	20.8	22.7	24.7
Water	26.2	28.4	37.9	30.4	29.3	36.0
Ligand						
3PG	—	—	28.7	18.7	29.2	41.6
Glycerol	—	—	49.0	—	—	—
Sulfate	21.1	—	—	—	—	—
R.m.s.d. from ideal						
Bond length (Å)	0.005	0.006	0.007	0.008	0.012	0.01
Bond angle (°)	0.8	0.8	1.0	0.9	1.4	1.2
Residues in Ramachandran plot (%)						
Most allowed	95.2	93.8	94.0	94.2	93.6	93.6
Allowed	4.8	6.0	5.5	5.7	6.0	6.2
Generously allowed	0.0	0.2	0.4	0.1	0.4	0.2
Disallowed	0.0	0.0	0.0	0.0	0.0	0.0
PDB code	2vfd	2vff	2vfe	2vfg	2vfi	2vfh

† R factor/R_{free} = $\sum_{hkl} |F_{obs} - F_{calc}| / \sum_{hkl} |F_{obs}|$, where F_{obs} and F_{calc} are the observed and calculated structure factors; 5% of the reflections were included in the test set for the calculation of R_{free}.

Table 4
Ligand binding and loop status in PfTIM and F96 mutant data sets.

Data set	Soaked/cocrystallized	Ligand concentration (m*M*)	No. of subunits per ASU	Active-site ligand	Interface ligand	Loop status
F96S, unliganded	Cocrystallized	50	2	No	No	Open
F96H, unliganded	Cocrystallized	50	2	No	No	Open
F96S, liganded	Cocrystallized, soaked	50, 100	2	No	Yes	Open
F96H, liganded	Cocrystallized, soaked	50, 100	4	No	Yes	Open
F96W, liganded	Cocrystallized	50	2	Yes	No	Closed in *A*, open and closed in *B*
WT–3PG	Cocrystallized, soaked	50, 100	2	Yes	Yes	Closed

which is in sharp contrast to previous studies with wild-type PfTIM in the presence of 3PG, which resulted in a ligand-bound active site with an open loop 6 (Parthasarathy, Balaram *et al.*, 2002). Sulfates and glycerol were modelled at the active site in the F96S mutant and 3PG-soaked F96S mutant structures, respectively. A sulfate with lower occupancy was modelled because the observed density showed a clear tetrahedral character and fitting water molecules led to unexplained blobs of residual density during refinement. The presence of sulfate is plausible since the protein purification involved a step of ammonium sulfate precipitation, while glycerol was used as a cryoprotectant. Interestingly, well defined electron density for the ligand was observed in the F96W mutant cocrystallized with 3PG. In the crystal structure of the F96W–3PG complex, the active-site loop 6 was closed in one subunit. In the other subunit, both open and closed conformations were observed with occupancies of 0.6 and 0.4, respectively. The conformation of Trp96 is different in the *A* and *B* subunits and these conformations match those of Phe96 in the open and closed states observed in previous PfTIM structures.

Attempts to soak the F96S and F96H mutants in a high concentration of 3PG resulted in the completely unexpected observation of ligand binding at the dimer interface. A similar treatment of wild-type PfTIM cocrystallized with 3PG resulted in a structure with full occupancy of the ligand at the active site and loop 6 in a closed conformation. Most importantly, one ligand molecule per subunit was also bound at the dimer interface. The results obtained in terms of loop status and ligand binding for the wild type and mutants are summarized in Table 4.

3.3. Ligand binding and active-site hydration

3PG was observed in the active site of the structures of the wild-type PfTIM in the loop-closed state and of the F96W mutant. A superposition of the structures shows that the phosphate position of 3PG depends on the loop 6 conforma-

tion (Fig. 2). The position of the phosphate remains relatively invariant for the ligand bound in the loop-closed state, while considerable variability is observed in the phosphate position in loop-open structures. This observation is consistent with the previous observation that loop closure is important for maintaining the position of the ligand for optimal activity (Parthasarathy, Ravindra *et al.*, 2002). The conformation of the triose segment of the bound molecule is variable (Fig. 2).

In the F96S and F96H mutant structures, the ligand did not bind at the active site on cocrystallization or on soaking at high concentration. A comparison of the residues at the active sites of the F96S and F96H mutants with those of the wild-type structure (Fig. 3) did not show any major differences in the conformations of the residues. Therefore, the observed differences could be a consequence of the water structure at the active site.

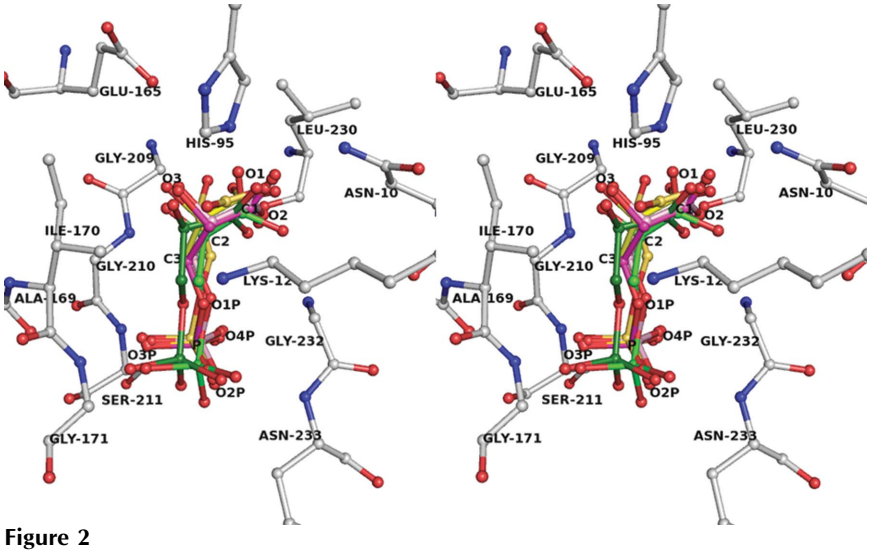

Figure 2
Superposition of 3PG bound in various PfTIM structures. 3PG molecules in the *A* and *B* subunits of the wild-type loop-open structure (green; PDB code 1m7o), the F96W mutant (magenta) and the wild-type loop-closed structure (yellow) are shown. The 3PG molecules in the two subunits are shown in dark and light shades. The residues in the vicinity of the active site are shown in grey. The residues and the atoms of 3PG are labelled. This figure was prepared in wall-eyed stereo using *PyMOL* (DeLano, 2002).

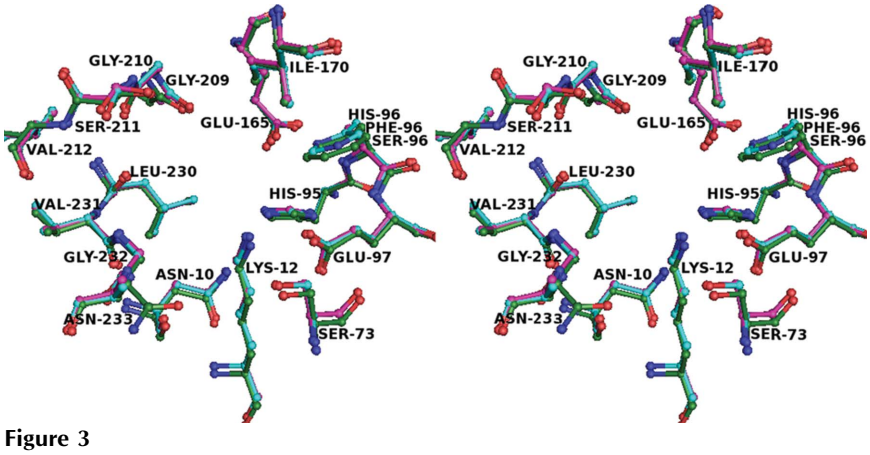

Figure 3
Superposition of the active site showing the residue conformations of F96S (pink), F96H (cyan) and wild-type PfTIM (green; PDB code 1ydv) in the unliganded structures. This figure was prepared in wall-eyed stereo using *PyMOL* (DeLano, 2002).

The hydration at the active sites of the F96S, F96H and F96W mutant structures and in the unliganded and ligand-bound wild-type structures was compared. Structures of a comparable resolution of between 1.95 and 2.25 Å were used in the analysis, with the exception of the unliganded F96S structure, which is at 1.4 Å resolution. In the F96S and F96H mutants the stretch of water molecules extending from the polar residue at position 96 to Ser73 can hinder entry of the ligand into the active site. These water molecules are in turn connected to water molecules at positions that overlap with the position of the ligand 3PG. Hence, expulsion of these water molecules is necessary for ligand binding. This water network is absent in the active sites of wild-type PfTIM and the F96W mutant, in which ligand binding has been observed. The water molecules implicated in the loss of affinity for the ligand at the active site have well defined density in the crystal structures of the mutants and their *B* factors are in the range of the mean *B* factors of the respective structures (Table 3).

The water structure at the active site of the mutants was also compared with that of TIM structures from other organisms. TIM structures at resolutions of better than of 2.3 Å were chosen. The highest resolution wild-type structure from each organism was selected and both unliganded structures and structures with various ligands (including sulfate or phosphate ions) were considered. A list of the structures used in the analysis is given in Table 5. The analysis confirmed that the water network connecting residue 96 and residue 73 of the adjacent subunit is weakened by the occurrence of a hydrophobic residue at either position 96 or 73 and the consequent absence of an anchoring hydrogen bond to the water molecule near the hydrophobic residue in wild-type TIMs. Ligands such as sulfate, phosphate and glycerol, which are bound despite the presence of the water network, bind in the place of the phosphate group of the substrate. Hence, the displacement of the water molecules at the triose end of the substrate is affected by the presence of the interconnecting water molecules, thus affecting the binding of the substrate or substrate analogue.

3.4. Ligand binding at the interface

An interesting observation during the crystallographic analysis of the mutants was the presence of the ligand at the dimer interface of PfTIM. The electron density of the ligand bound at the interface is shown in Fig. 4(*a*). The ligand binding at the interface occurs in a similar manner in the mutants

Table 5
List of TIM structures included in the analysis of water structure at the active site.

PDB code	Resolution (Å)	Source	Ligand ID (as in PDB)
1mo0	1.7	*Caenorhabditis elegans*	SO4, ACT
1m6j	1.5	*Entamoeba histolytica*	
1tph	1.8	*Gallus gallus*	PGH
2dp3	2.1	*Giardia lamblia*	SO4
2jgq	2.3	*Helicobacter pylori*	QGA, PO4
2jk2	1.7	*Homo sapiens*	
1n55	0.83	*Leishmania mexicana*	GOL, ACY, PGA
1if2	2	*L. mexicana*	129
1r2r	1.5	*Oryctolagus cuniculus*	TRS, DMS, MG
1r2t	2.25	*O. cuniculus*	
1ney	1.2	*Saccharomyces cerevisiae*	13P
1i45	1.8	*S. cerevisiae*	
7tim	1.9	*S. cerevisiae*	PGH
2i9e	2	*Tenebrio molitor*	TRS
1yya	1.6	*Thermus thermophilus*	PO4, NA
1tpf	1.8	*Trypanosoma brucei brucei*	DMS
1iih	2.2	*T. brucei brucei*	3PG
1tcd	1.83	*T. cruzi*	
2oma	2.15	*T. cruzi*	SO4, PGE, PEG
1o5x	1.1	*Plasmodium falciparum*	2PG, 3PY, PO3
1lyx	1.9	*P. falciparum*	PGA
1ydv	2.2	*P. falciparum*	

and the wild-type protein. Two molecules of 3PG are bound at the interface, bridged by two water molecules. The two water molecules are present on the twofold relating the monomers of the dimeric TIM. Each 3PG has contacts from both the subunits of PfTIM, the majority being from one of the subunits. The contacts involved in holding the ligand in place are shown in Fig. 4(*b*), together with a comparison with the unliganded interface (Fig. 4*c*; PDB code 1o5x). The side chains of Lys68 and Asp108 and the main-chain atoms of Phe102 and His103 are involved in contacts at the triose part of the ligand. The C^{α} position of His103 changes on 3PG binding. In addition, the imidazole rings of His103 from the *A* and *B* subunits form a stacking interaction (Fig. 4*d*) and the N^{ε} atom makes a hydrogen bond to the ligand bound to the neighbouring subunit. The phosphate group is held in place by residues Lys112, Arg98, Asn65 and Glu104 and water molecules. Glu104, which occurs in alternate conformations in many of the PfTIM structures with an unliganded interface, selectively adopts one of the conformations such that ligand binding at the interface is facilitated. The binding pocket occurs towards the outer portion of the interface (Fig. 4*a*). This region is identified as a cavity in the native PfTIM dimer (PDB code 1ydv) with a volume of 13 $Å^3$. Only one water molecule at the phosphate position is displaced per ligand molecule upon binding at the interface.

3.5. Loop closure and crystal contacts

In wild-type PfTIM, a loop-closed structure was obtained on soaking the crystals with excess ligand, suggesting that loop closure takes place without significant changes in the crystal structure. To examine the possibilities of loop movement in the crystalline state, a detailed comparison between the crystal contacts of wild-type PfTIM complexed with 3PG in the loop-open and loop-closed structures was carried out. Analysis of the crystal contacts shows that loop 6 is in the vicinity of crystallographically related subunits. In the loop-open form, Gly173 of the *B* subunit interacts with Asn233 of the *A* subunit of the dimer related by unit translation along the *b* axis, while in the loop-closed form Lys237 of the *A* subunit makes contacts with Gly171 and Thr172 of the *B* subunit of the dimer related by a similar translation. These are minor contacts. However, the remainder of the contacts across the same interface, involving Thr16*A*, Glu18*A* and Ser19*A* with Glu215*B* and Glu238*A* with Lys237*B*, are maintained irrespective of the loop position. The residues involved in the contacts with loop 6, Asn233 and Lys237, are flexible. Their side chains have not been modelled consistently in many other PfTIM structures. Hence, the loop status is not dictated by the crystal packing and the space available for the loop at the interface allows facile interconversion of the open and closed forms. Instances of cell change on crystal soaking have been reported previously for chicken TIM (Banner *et al.*, 1976). In the case of yeast TIM soaked in DHAP, a visible change in crystal morphology following cell change has also been observed (Jogl *et al.*, 2003).

4. Discussion

4.1. Ligand binding at the active site

The kinetic data (Table 1) show a decreased catalytic efficiency for the mutants, as well as a decreased affinity for substrates and inhibitors. With the exception of F96W, none of the cocrystallization or soaking trials resulted in crystals of mutant PfTIMs with ligand (inhibitor) bound at the active site. The reduction in the catalytic rate of the F96W mutant is less than that of the F96S and F96H mutants. The crystal structure of the 3PG-bound form of the F96W mutant obtained by cocrystallization shows an increased propensity for the closed state of the loop. The higher propensity for loop closure in the F96W mutant can be rationalized in terms of a larger number of van der Waals contacts between the indole ring of Trp96 and the loop residue Leu167 in the closed state. This can in principle affect the rate of loop opening and closing and hence slow product release, leading to a decrease in the catalytic rate.

The isomerization reaction catalyzed by TIM involves a process in which the Glu165 carboxylic acid side chain functions as the catalytic base in its anionic form and abstracts a proton from the substrate. In the subsequent step, the protonated carboxylic group functions as the proton donor, delivering the proton to the same face of the enediol intermediate and resulting in the formation of D-GAP from the achiral DHAP (Raines & Knowles, 1986; Raines *et al.*, 1986; Straus *et al.*, 1985; Cui & Karplus, 2002; Bash *et al.*, 1991). Such a finely tuned proton-transfer process will be facilitated by the exclusion of water from the immediate vicinity of the reactive functionalities.

The role of water in maintaining the catalytic efficiency of TIM has been considered previously (Zhang *et al.*, 1999). In the unliganded structures, water molecules are present at the

positions corresponding to the O atoms of 3PG. Ligand binding at the active site is accompanied by displacement of water molecules, as can be observed from Fig. 5(*a*), which shows a superposition of the unliganded (PDB code 1ydv; 2.2 Å resolution) and ligand-bound (PDB code 1m7o; 2.4 Å resolution) structures of wild-type PfTIM. Closure of loop 6 leads to further expulsion of water molecules from the active site. The superposition of the loop-open and loop-closed structures of PfTIM with the bound ligand 3PG highlights the water molecules that are displaced on loop closure (Fig. 5*b*). Previous studies on rabbit TIM (Aparicio *et al.*, 2003) have shown that a number of water molecules are displaced on ligand binding and loop closure. A water molecule essential for activity is also associated with the catalytic Glu165, which changes from a swung-in to a swung-out position during catalysis (Zhang *et al.*, 1999). The structure of the S96P mutant

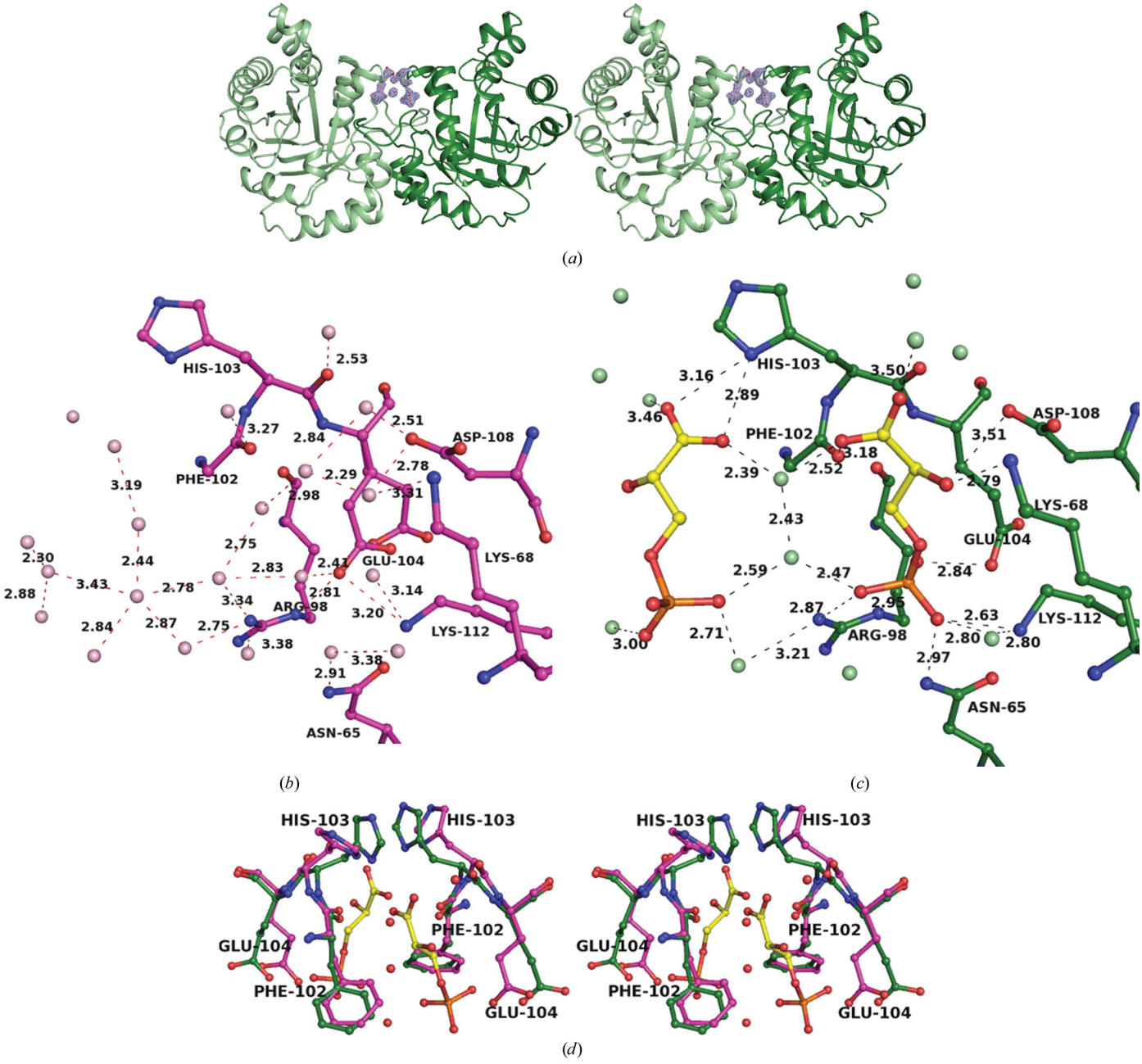

Figure 4
Ligand binding at the dimer interface. (*a*) TIM dimer with 3PG bound at the interface. Electron density (simulated-annealing $F_o - F_c$ omit map contoured at 2.5σ) for the ligand bound at the interface in the F96H mutant is shown. The two subunits are coloured in different shades. This figure was prepared in wall-eyed stereo using *PyMOL* (DeLano, 2002). (*b*) Interactions at the unliganded interface (PDB code 1o5x). The residues are shown in ball-and-stick representation and the water molecules are shown as spheres. The hydrogen-bonding distances are labelled. (*c*) Interactions of bound 3PG at the interface. The bound 3PG molecules are shown in yellow. (*d*) Difference in the main chain at His103 in the interface-bound (green) and unbound (magenta) forms of PfTIM. A stacking interaction between the histidines can be observed in the 3PG-bound structure. This figure was prepared in wall-eyed stereo using *PyMOL* (DeLano, 2002).

of yeast TIM suggests that the mutation affects the activity because of the removal of a water molecule attached to the backbone N atom of residue 96 (Zhang *et al.*, 1999).

The occurrence of a strong water network that can hinder ligand binding in the F96S and F96H mutants could be a consequence of the presence of hydrophilic residues at both residue positions 96 and 73. The overwhelming majority of TIM sequences possess the Ala73/Ser96 pair, while the plasmodial sequences contain the Ser73/Phe96 pair. The selection of compensatory mutations during evolution appears to be a consequence of the pressure to maintain active-site hydration at an optimal level. Thus, a combination of hydrophobic and hydrophilic residues at the two positions is maintained in TIM, such that the water molecules can be displaced with relative ease to make way for the ligand. The role of the water network in ligand binding needs to be further probed by experiments with an F96S/S73A double mutant of PfTIM.

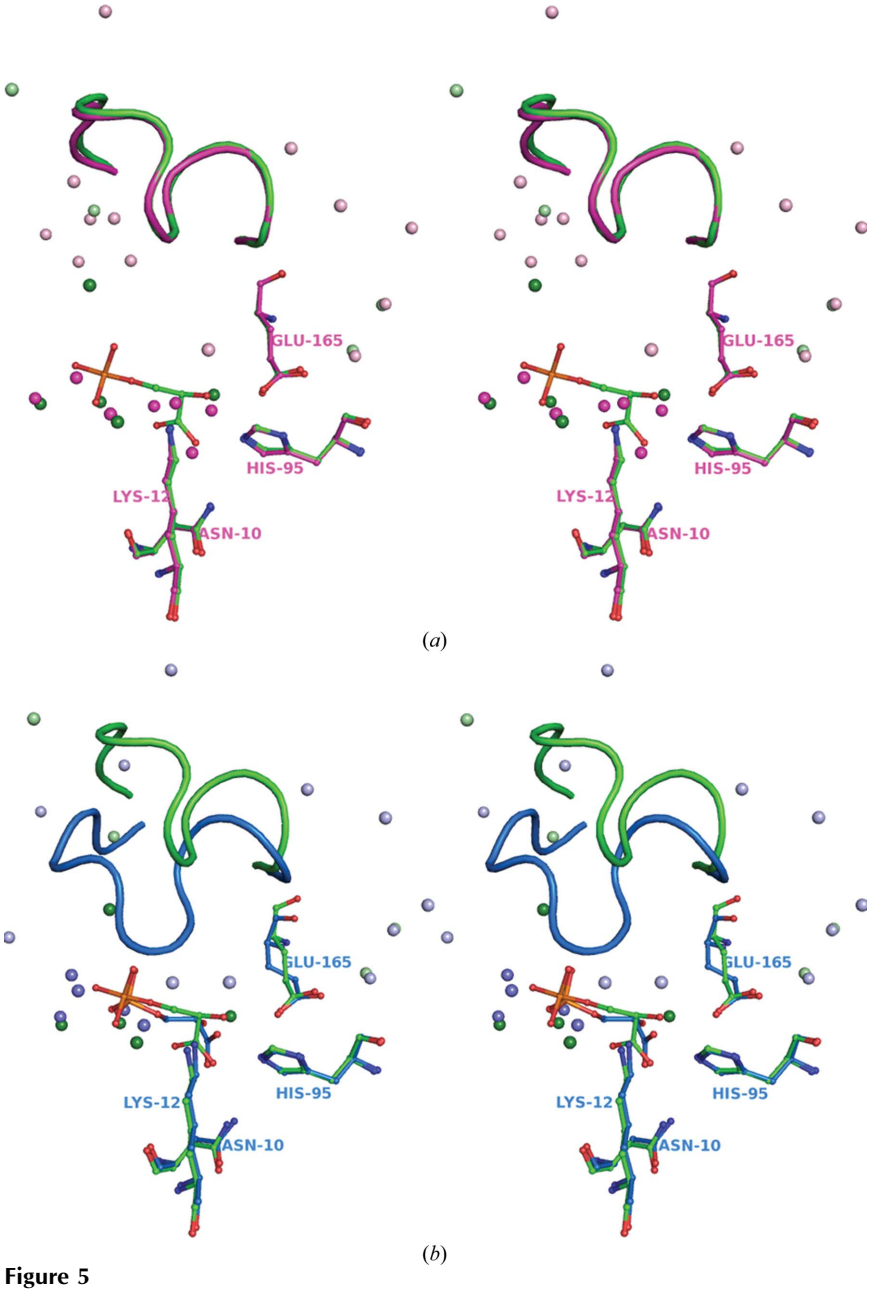

Figure 5
Changes in the water structure at the active site accompanying ligand binding and loop closure. Loop 6 is shown in cartoon representation, while the active-site residues are shown in ball-and-stick representation. The respective water molecules are shown as spheres in the corresponding colours. The water molecules in the neighbourhood (<4 Å) of the loop residues are shown in a lighter shade compared with the water molecules within 4 Å of the bound ligand at the active site. All the water molecules shown in the figure have been included during structure solution on observation of electron density corresponding to $2F_o - F_c$ at the 1σ level or $F_o - F_c$ at the 3σ level following refinement. The figures were prepared in wall-eyed stereo using *PyMOL* (DeLano, 2002). (*a*) Superposition of the unliganded wild-type PfTIM structure (magenta; PDB code 1ydv; 2.2 Å resolution) and the wild-type PfTIM–3PG complex with loop open (green; PDB code 1m7o; 2.4 Å resolution). (*b*) Superposition of the wild-type PfTIM 3PG-bound structures with loop open (green; PDB code 1m7o; 2.4 Å resolution) and loop closed (blue; PDB code 2vfi; 2.25 Å resolution).

4.2. Ligand binding at the interface

An unexpected result of the present study is the observation of binding of the 3PG ligand at a well defined site at the dimer interface. This is the first example of crystallographic characterization of the binding of a triose phosphate inhibitor at the interface. Of the residues involved in binding the ligand at the interface, Asn65, Arg98, Glu104 and Lys112 are conserved in TIMs from other species, Phe102 and His103 are not conserved but interact with 3PG through main-chain atoms and Lys68 and Asp108 are not conserved (Fig. 6*a*). Hence, it is possible that the ligand/substrate can also bind at the interface in several other TIMs. There have been previous reports from docking studies that benzothiazoles may interact favourably with the aromatic patch at the dimer interface (Espinoza-Fonseca & Trujillo-Ferrara, 2005). The crystal structure of *T. cruzi* TIM complexed with 3-(2-benzothiazolylthio)-1-propanesulfonic acid shows the ligand bound near the interface (Tellez-Valencia *et al.*, 2004). The observed site of binding differs from that reported in the present study for 3PG. Organic solvent molecules have also been shown to occupy positions in the dimer interface, as observed in the crystal structure of *T. cruzi* TIM soaked in hexane (Gao *et al.*, 1999).

An interesting feature of 3PG binding to the two distinct sites in PfTIM is the marked difference in the nature of the interactions made by the negatively charged phosphate group. At the active site, there appears to be very little electrostatic anchoring of the phosphate, as seen from the structures of several TIM ligand complexes. Indeed, the

three phosphate O atoms form hydrogen bonds to neutral donors, namely the main-chain amides of Ser211, Gly232 and Gly171, the side-chain OH of Ser211 and water molecules (numbering according to PfTIM; Fig. 6*b*). The only charged group in the vicinity is the ε-amino group of Lys12, which approaches the phosphate ester O atom (N—O distance of 3.4 Å; Fig. 6*b*). In contrast, the ligand-binding site at the interface reveals that the phosphate group is anchored by two positively charged residues, Arg98 and Lys112, both of which make hydrogen bonds to two of the phosphate O atoms (OC2···Arg98 NH2, 2.87 Å; OC3···Lys112 NZ, 2.63 Å; Fig. 6*c*). Additionally, the third phosphate O atom approaches two potential hydrogen-bond donors Asn65 and Glu104, which are two highly conserved residues in TIMs. Glu104 is essential for maintenance of the dimer interface in TIM owing to a conserved water network of buried water molecules that bridges the two subunits (Rodríguez-Almazán *et al.*, 2008). The formation of a hydrogen bond would require Glu104 to be protonated. This is feasible as the soaking experiments were carried out at pH 5.0.

Can ligand binding at the interface of PfTIM have any biochemical significance? The possible physiological relevance of methylglyoxal formation by naturally occurring TIM mutants identified in drosophila (Gnerer *et al.*, 2006) provides fresh input for the examination of the mechanistic basis of the phosphate-elimination reaction. The striking differences between the protein–ligand contacts at the two sites raise the question whether the interface site could indeed facilitate the undesired phosphate-elimination reaction. Previous studies have indeed demonstrated that chicken TIM converts DHAP to methylglyoxal by phosphate elimination (Campbell *et al.*, 1979). Further studies of specifically designed TIM mutants and comparisons with methylglyoxal synthase (Saadat & Harrison, 1998, 1999, 2000; Marks *et al.*, 2001) are necessary in order to establish whether the additional binding site reported in the present study is of relevance in understanding the undesired elimination reaction that leads to the toxic metabolite methylglyoxal.

Before the structures reported in this communication became available, it was assumed that the S96F mutation that is exclusively observed in *P. falciparum* TIM merely influences the loop dynamics. However, the structures reported here illustrate that Phe96 of PfTIM plays a crucial role in both ligand binding and loop movement. The presence of Phe96 and Leu167 facilitates the occurrence of the loop-open state of PfTIM, while retention of the ligand in the TIM with increased probability of the loop-open state is controlled by water-mediated interactions involving Ser73 and Asn233. Thus, residues Phe96,

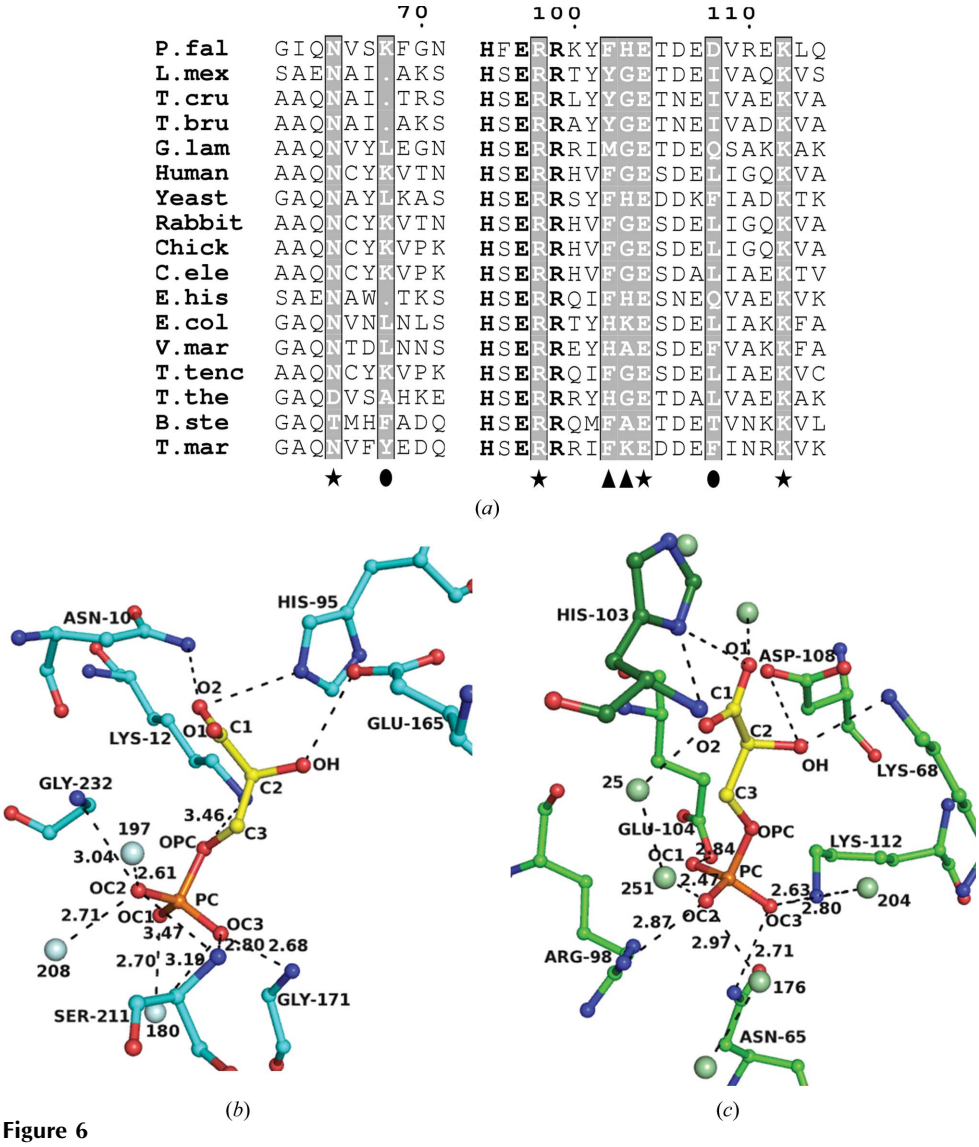

Figure 6
(*a*) Conservation of residues involved in binding 3PG at the dimer interface. The residues involved in 3PG binding are highlighted. Conservation is denoted by the symbols at the base of the alignment: stars for conserved residues, triangles for nonconserved residues involved in backbone interactions with 3PG and circles for nonconserved residues. The alignment was generated by a structure-based sequence alignment of all TIM structures using *MUSTANG* (Konagurthu *et al.*, 2006) and represented using *ESPript* (Gouet *et al.*, 1999). Other residues conserved with 100% identity are shown in bold letters. The residue numbering shown at the top of the alignment correspond to PfTIM. (*b*) 3PG bound at the active site of PfTIM in the loop-closed state. (*c*) 3PG bound at the interface of PfTIM. His103 from the adjacent subunit involved in binding of the ligand is shown in a darker shade.

Ser73, Leu167 and Asn233, all of which are unique to PfTIM, have been chosen by natural selection to maintain the catalytic efficiency of triosephosphate isomerase in *P. falciparum*.

This research was supported by program grants from the Council for Scientific and Industrial Research (CSIR), Department of Biotechnology (DBT), Department of Science and Technology (DST), Government of India. PG and MB acknowledge CSIR for Senior Research Fellowships. We thank Dr Lokanath and the beamline staff at BL44XU for assistance during data collection of the F96S data set. PG and MRNM thank Professor T. Tsukihara, Institute of Protein Research, Osaka University and Professor N. Kunishima, RIKEN SPring-8 Center, Harima Institute for a travel grant to Japan. This work was performed under the international collaborative research program of the Institute of Protein Research, Osaka University. We thank the staff of the X-ray Laboratory, Molecular Biophysics Unit, Indian Institute of Science for their cooperation during the course of the investigations. The mass-spectrometric facility was supported under the Proteomics program of the Department of Biotechnology, Government of India.

References

Alber, T. C., Banner, D. W., Bloomer, A. C., Petsko, G. A., Phillips, D., Rivers, P. S. & Wilson, I. A. (1981). *Philos. Trans. R. Soc. London Ser. B*, **293**, 159–171.

Alber, T. C., Davenport, R. C. Jr, Giammona, D. A., Lolis, E., Petsko, G. A. & Ringe, D. (1987). *Cold Spring Harb. Symp. Quant. Biol.* **52**, 603–613.

Albery, W. J. & Knowles, J. R. (1976*a*). *Biochemistry*, **15**, 5588–5600.

Albery, W. J. & Knowles, J. R. (1976*b*). *Biochemistry*, **15**, 5627–5631.

Albery, W. J. & Knowles, J. R. (1976*c*). *Biochemistry*, **15**, 5631–5640.

Albery, W. J. & Knowles, J. R. (1977). *Angew. Chem. Int. Ed. Engl.* **16**, 285–293.

Anderson, A. & Cooper, R. A. (1970). *J. Gen. Microbiol.* **62**, 329–334.

Aparicio, R., Ferreira, S. T. & Polikarpov, I. (2003). *J. Mol. Biol.* **334**, 1023–1041.

Banner, D. W., Bloomer, A., Petsko, G. A., Phillips, D. C. & Wilson, I. A. (1976). *Biochem. Biophys. Res. Commun.* **72**, 146–155.

Bash, P. A., Field, M. J., Davenport, R. C., Petsko, G. A., Ringe, D. & Karplus, M. (1991). *Biochemistry*, **30**, 5826–5832.

Brunger, A. T. (2007). *Nature Protoc.* **2**, 2728–2733.

Brünger, A. T., Adams, P. D. & Rice, L. M. (1997). *Structure*, **5**, 325–336.

Campbell, I. D., Jones, R. B., Kiener, P. A. & Waley, S. G. (1979). *Biochem. J.* **179**, 607–621.

Collaborative Computational Project, Number 4 (1994). *Acta Cryst.* D**50**, 760–763.

Cui, Q. & Karplus, M. (2002). *J. Am. Chem. Soc.* **124**, 3093–3124.

DeLano, W. L. (2002). *The PyMOL Molecular Graphics System.* DeLano Scientific, San Carlos, California, USA.

Derreumaux, P. & Schlick, T. (1998). *Biophys. J.* **74**, 72–81.

Emsley, P. & Cowtan, K. (2004). *Acta Cryst.* D**60**, 2126–2132.

Espinoza-Fonseca, L. M. & Trujillo-Ferrara, J. G. (2005). *Biochem. Biophys. Res. Commun.* **328**, 922–928.

Gao, X. G., Maldonado, E., Perez-Montfort, R., Garza-Ramos, G., de Gomez-Puyou, M. T., Gomez-Puyou, A. & Rodriguez-Romero, A. (1999). *Proc. Natl Acad. Sci. USA*, **96**, 10062–10067.

Gnerer, J. P., Kreber, R. A. & Genetzky, B. (2006). *Proc. Natl Acad. Sci. USA*, **103**, 14987–14993.

Gouet, P., Courcelle, E., Stuart, D. I. & Métoz, F. (1999). *Bioinformatics*, **15**, 305–308.

Jogl, G., Rozovsky, S., McDermott, A. E. & Tong, L. (2003). *Proc. Natl Acad. Sci. USA*, **100**, 50–55.

Joseph, D., Petsko, G. A. & Karplus, M. (1990). *Science*, **249**, 1425–1428.

Kleywegt, G. J. & Jones, T. A. (1994). *Acta Cryst.* D**50**, 178–185.

Knowles, J. R. (1991). *Nature (London)*, **350**, 121–124.

Konagurthu, A. S., Whisstock, J. C., Stuckey, P. J. & Lesk, A. M. (2006). *Proteins*, **64**, 559–574.

Kreitsch, W. K., Pentchev, P. G., Klingenburg, H., Hofstatter, T. & Bucher, T. (1970). *Eur. J. Biochem.* **14**, 289–300.

Krissinel, E. & Henrick, K. (2004). *Acta Cryst.* D**60**, 2256–2268.

Marks, G. T., Harris, T. K., Massiah, M. A., Mildvan, A. S. & Harrison, D. H. (2001). *Biochemistry*, **40**, 6805–6818.

Murshudov, G. N., Vagin, A. A. & Dodson, E. J. (1997). *Acta Cryst.* D**53**, 240–255.

Oesper, P. & Meyerhof, O. (1950). *Arch. Biochem.* **27**, 223–233.

Parthasarathy, S., Balaram, H., Balaram, P. & Murthy, M. R. N. (2002). *Acta Cryst.* D**58**, 1992–2000.

Parthasarathy, S., Eaazhisai, K., Balaram, H., Balaram, P. & Murthy, M. R. (2003). *J. Biol. Chem.* **278**, 52461–52470.

Parthasarathy, S., Ravindra, G., Balaram, H., Balaram, P. & Murthy, M. R. (2002). *Biochemistry*, **41**, 13178–13188.

Plaut, B. & Knowles, J. R. (1972). *Biochem. J.* **129**, 311–320.

Pompliano, D. L., Peyman, A. & Knowles, J. R. (1990). *Biochemistry*, **29**, 3186–3194.

Putman, S. J., Coulson, A. F., Farley, I. R., Riddleston, B. & Knowles, J. R. (1972). *Biochem. J.* **129**, 301–310.

Raines, R. T. & Knowles, J. R. (1986). *Ann. NY Acad. Sci.* **471**, 266–271.

Raines, R. T., Sutton, E. L., Straus, D. R., Gilbert, W. & Knowles, J. R. (1986). *Biochemistry*, **25**, 7142–7154.

Ranie, J., Kumar, V. P. & Balaram, H. (1993). *Mol. Biochem. Parasitol.* **61**, 159–169.

Richard, J. P. (1991). *Biochemistry*, **30**, 4581–4585.

Rieder, S. V. & Rose, I. A. (1959). *J. Biol. Chem.* **234**, 1007–1010.

Rodríguez-Almazán, C., Arreola, R., Rodríguez-Larrea, D., Aguirre-López, B., de Gómez-Puyou, M. T., Pérez-Montfort, R., Costas, M., Gómez-Puyou, A. & Torres-Larios, A. (2008). *J. Biol. Chem.* **283**, 23254–23263.

Rose, I. A. (1962). *Brookhaven Symp. Biol.* **15**, 293–309.

Rozovsky, S., Jogl, G., Tong, L. & McDermott, A. E. (2001). *J. Mol. Biol.* **310**, 271–280.

Rozovsky, S. & McDermott, A. E. (2001). *J. Mol. Biol.* **310**, 259–270.

Saadat, D. & Harrison, D. H. (1998). *Biochemistry*, **37**, 10074–10086.

Saadat, D. & Harrison, D. H. (1999). *Structure*, **7**, 309–317.

Saadat, D. & Harrison, D. H. (2000). *Biochemistry*, **39**, 2950–2960.

Sarkar, G. & Sommer, S. S. (1990). *Biotechniques*, **8**, 404–407.

Straus, D., Raines, R., Kawashima, E., Knowles, J. R. & Gilbert, W. (1985). *Proc. Natl Acad. Sci. USA*, **82**, 2272–2276.

Sun, J. & Sampson, N. S. (1998). *Protein Sci.* **7**, 1495–1505.

Sun, J. & Sampson, N. S. (1999). *Biochemistry*, **38**, 11474–11481.

Tellez-Valencia, A., Olivares-Illana, V., Hernandez-Santoyo, A., Perez-Montfort, R., Costas, M., Rodriguez-Romero, A., Lopez-Calahorra, F., Tuena de Gomez-Puyou, M. & Gomez-Puyou, A. (2004). *J. Mol. Biol.* **341**, 1355–1365.

Verlinde, C. L., Witmans, C. J., Pijning, T., Kalk, K. H., Hol, W. G., Callens, M. & Opperdoes, F. R. (1992). *Protein Sci.* **1**, 1578–1584.

Williams, J. C. & McDermott, A. E. (1995). *Biochemistry*, **34**, 8309–8319.

Zhang, Z., Komives, E. A., Sugio, S., Blacklow, S. C., Narayana, N., Xuong, N. H., Stock, A. M., Petsko, G. A. & Ringe, D. (1999). *Biochemistry*, **38**, 4389–4397.